RESEARCH ARTICLE

Adrian Pittari · Ray A. F. Cas · Joe J. Monaghan ·
Joan Martí

Instantaneous dynamic pressure effects on the behaviour of lithic boulders in pyroclastic flows: the Abrigo Ignimbrite, Tenerife, Canary Islands

Abstract A method for estimating the instantaneous dynamic pressure near the base of ancient pyroclastic flows, using large lithic boulders from the late Pleistocene Abrigo Ignimbrite, is proposed here. The minimum instantaneous dynamic pressure is obtained by determining the minimum aerodynamic drag force exerted by a pyroclastic flow onto a stationary boulder that will allow the boulder to overcome static friction with the underlying substrate, and move within the flow. Consideration is given to the properties of the boulder (shape, roughness, size, density and orientation relative to the flow), substrate (type and hill slope angle), boulder-substrate interface (looseness of boulder, coefficient of static friction) and flow (coefficient of aerodynamic drag). Nineteen boulders from massive, lithic-rich ignimbrite deposits at two localities on Tenerife were assessed in this study. Minimum dynamic pressures required for Abrigo pyroclastic flows to move these boulders ranged from 5 to 38 kPa, which are comparable to dynamic pressures previously calculated from observations of the damage caused by recent pyroclastic flows. Considering the maximum possible range in flow density, the derived minimum velocity range for the Abrigo pyroclastic flows is 1.3 to 87 m s^{-1}.

A. Pittari (✉) · R. A. F. Cas
School of Geosciences, Monash University,
Victoria, 3800, Australia
e-mail: Adrian.Pittari@sci.monash.edu.au
Tel.: +61-3-99054885
Fax: +61-3-99054903

J. J. Monaghan
School of Mathematical Sciences, Monash University,
Victoria, 3800, Australia

J. Martí
Instituto de las Ciencias de la Tierra 'Juame Almera', CSIC,
Llius Solé Sabarís s/n,
08028 Barcelona, Spain

Introduction

Pyroclastic flows are highly destructive phenomena associated with explosive volcanic eruptions and are capable of flattening entire forests and destroying infrastructure. To understand the destructive power of a pyroclastic flow it is useful to determine dynamic pressure, which is the instantaneous pressure above background the flow exerts on an obstacle and is a function of the bulk flow density and horizontal velocity. The range of dynamic pressures of nuclear blasts and the relative damage they cause to infrastructure have been used as an analogy to assess the dynamic pressures within volcanic blasts and surges (Valentine 1998). Estimates of dynamic pressure within pyroclastic currents have been made based on the blow-down of trees and poles (e.g. Clarke and Voight 2000) and building damage (Nunziante et al. 2003; Baxter et al. 2005), or have been generated through numerical simulations (Valentine and Wohletz 1989; Esposti Ongaro et al. 2002). However, no previous attempt has been made to estimate dynamic pressures, as a basis for assessing the flow dynamics, of pre-historic pyroclastic flows from their deposit characteristics.

This study provides a new method of estimating the minimum instantaneous dynamic pressure within the basal zone of a pyroclastic flow based on the entrainment of large lithic boulders from the substrate. The lithic-rich Abrigo Ignimbrite deposit (Tenerife, Canary Islands) is ideal for this study. Large substrate-derived basalt boulders commonly occur within deposits of massive ignimbrite either as isolated clasts or within lithic concentration zones. The minimum force required to move these clasts is related to the minimum dynamic pressure. This provides a basis for an assessment of typical pyroclastic flow velocities and densities associated with the Abrigo pyroclastic flows.

Geological Setting

Early subaerial volcanism on the active oceanic island of Tenerife consisted firstly of a basaltic shield-building phase (>11.6–3.3 Ma) followed by the construction of the central largely phonolitic Las Cañadas edifice (3.8 to ~2 Ma; Fuster et al. 1968; Anchochea et al. 1990; Martí et al. 1994; Ablay and Kearey 2000). Since ~2 Ma multiple cycles of phonolitic explosive volcanism, each culminating in a climactic caldera-forming event, have dominated the Las Cañadas edifice and its summit caldera (Fig. 1; Martí et al. 1994). Subsequently, a complex sequence of pyroclastic deposits has been deposited onto the outer flanks of the edifice, and thick sequences are particularly preserved on the southern coastal plain (e.g. Bryan et al. 1998; Edgar 2003).

The moderate volume Abrigo Ignimbrite was deposited from the last major climactic caldera-forming eruption of the Las Cañadas edifice with independent $^{40}Ar/^{30}Ar$ ages ranging from 196 to 171 ka (Mitjavilla and Villa 1993; Nichols 2001; Brown et al. 2003). Outcrop exposure of the ignimbrite occurs on the lower slopes all around the island (Fig. 1), in both palaeovalleys and on the interfluves, and correlates to fines-poor, lithic breccia on the eastern caldera rim (Pittari 2004; Pittari and Cas 2004; Pittari et al. 2005, 2006). An underlying localised plinian fallout deposit has also been tentatively attributed to the same eruption (Pittari 2004; Pittari et al. 2006).

Extensive sheetlike ignimbrite deposits are best preserved on the southwestern to eastern coastal plains, where there are generally two major depositional units (Fig. 2a), the lower Sur-A unit (up to 18 m thick) and the upper Sur-C unit (up to 14 m thick), separated by a 1–3-cm-thick accretionary lapilli bearing ash layer (Pittari 2004; Pittari et al. 2005; 2006). Thick valley ponded deposits of the Sur-A and –C units generally consist of massive, lithic-rich (up to 40–50 vol%) ignimbrite, with an abundance of both vent-derived (syenitic, coherent basaltic to phonolitic volcanic, pyroclastic, epiclastic) and substrate-derived (mostly basaltic) lithic pebbles and cobbles. Large lithic cobbles and boulders are often scattered throughout the deposit or occur in discrete planar concentration zones of either (1) only substrate-derived lithic clasts (mono-/bilithologic), commonly in the lower part of the Sur-A unit, or (2) vent-derived lithic clasts (heterolithologic), particularly in the upper Sur-A unit (Fig 2a). Pumice clasts (~15–25 vol%) occur through the deposit but are more highly concentrated towards the top of the Sur-A unit or within lithic-poor, commonly stratified, facies and massive pumice-rich ignimbrite lobes (Pittari et al. 2005) in the lower Sur-C unit. Ignimbrite veneer deposits of the Sur-A and C units on the interfluves generally contain finer-grained and lower proportions of lithic clasts, and are stratified. Local stratigraphic and facies variations (see Fig. 2b and the next section) are common and are due to the local topography. Multiple depositional units of massive, lithic-rich rich ignimbrite are also exposed on the lower northern and western flanks of the Las Cañadas edifice.

Fig. 1 Map of Tenerife showing the preserved exposure of the Abrigo Ignimbrite, and the localities and their coordinates where large lithic boulders were examined for this study. (*Inset*) Location map of the Canary Islands
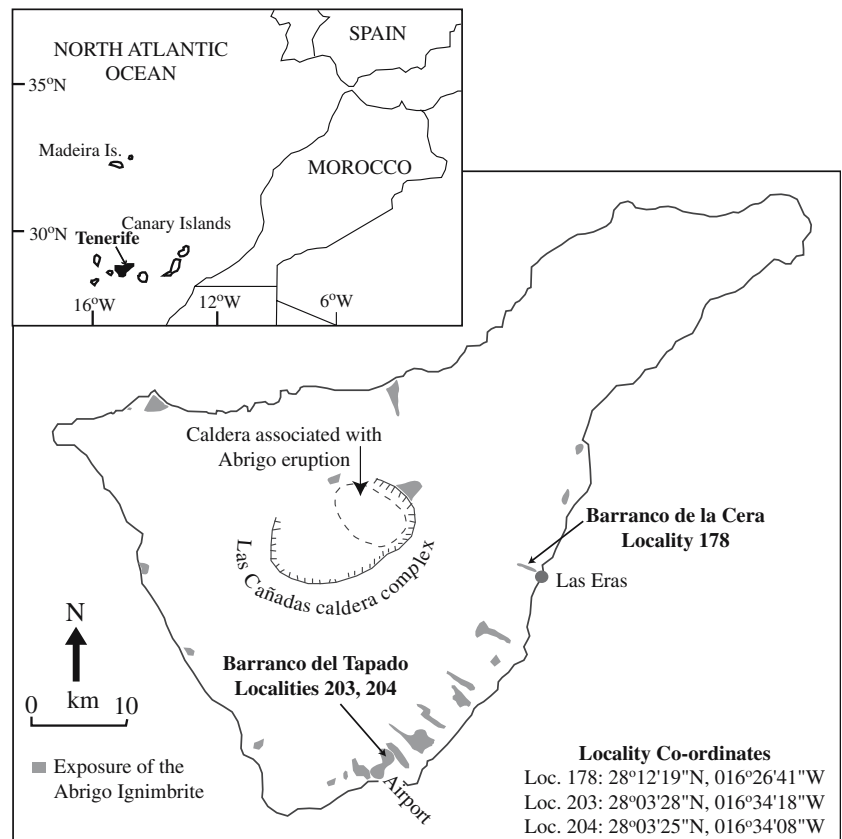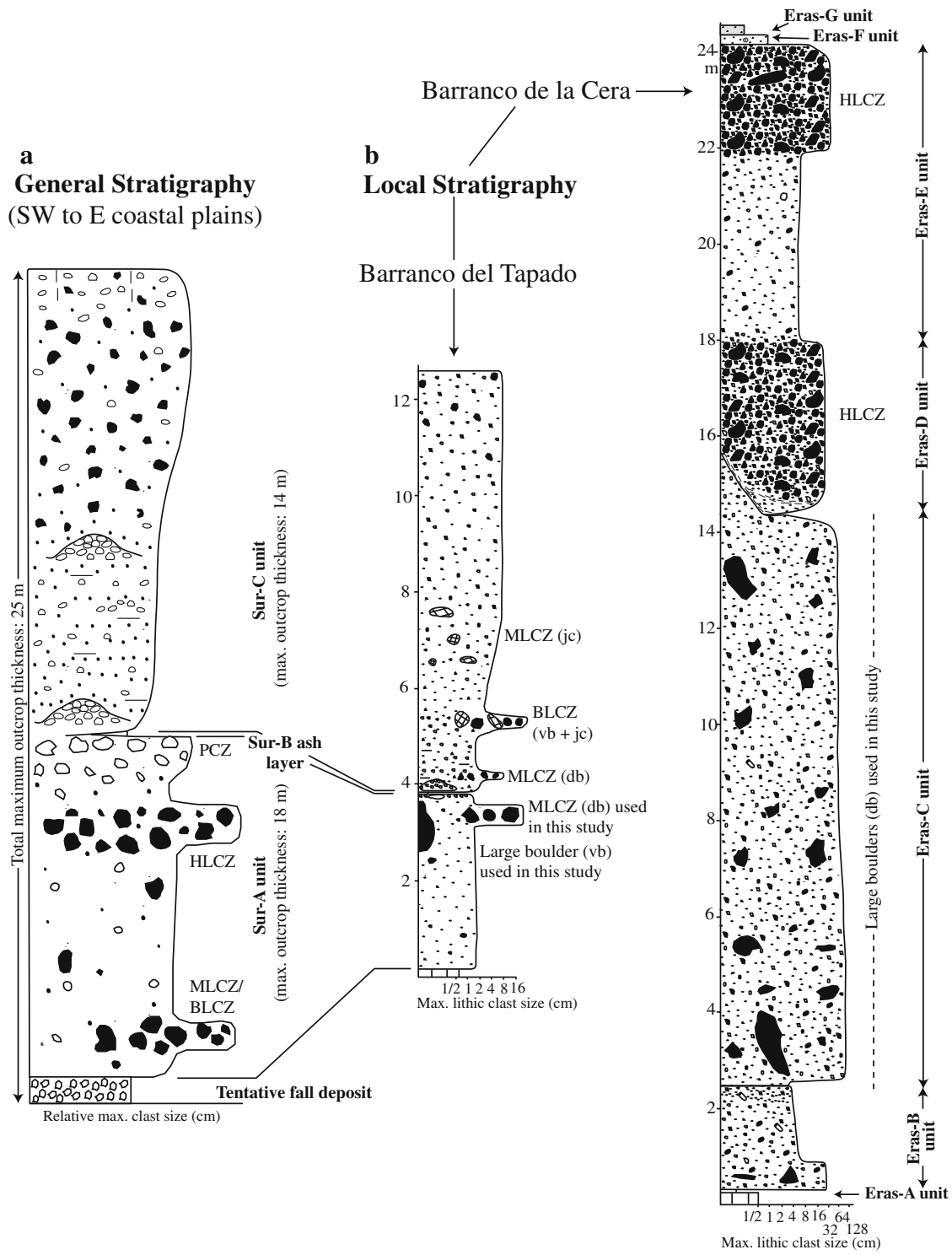
Fig. 2 a Simplified stratigraphy of the Abrigo Ignimbrite, and its tentative fall deposit, on the southwestern to eastern coastal plains. **b** Composite stratigraphic logs of valley ponded deposits in the barrancos del Tapado and de la Cera, representing the localities visited for this study. *HLCZ*, *BLCZ* and *MLCZ* are heterolithologic, bilithologic and monolithologic lithic concentration zones respectively; *PCZ* pumice concentration zone; *vb* vesicular basalt; *db* dense basalt; *jc* dense, glassy, juvenile clast

Site description

This study was conducted at two sites on the southern and eastern lower slopes of Tenerife. In the Barranco de la Cera,

2.5 km upstream from the coastal town of Las Eras (Loc. 178, Fig. 1), the Abrigo Ignimbrite has a maximum thickness of 25 m. The internal ignimbrite stratigraphy in this barranco (valley) differs from the generalised sequence
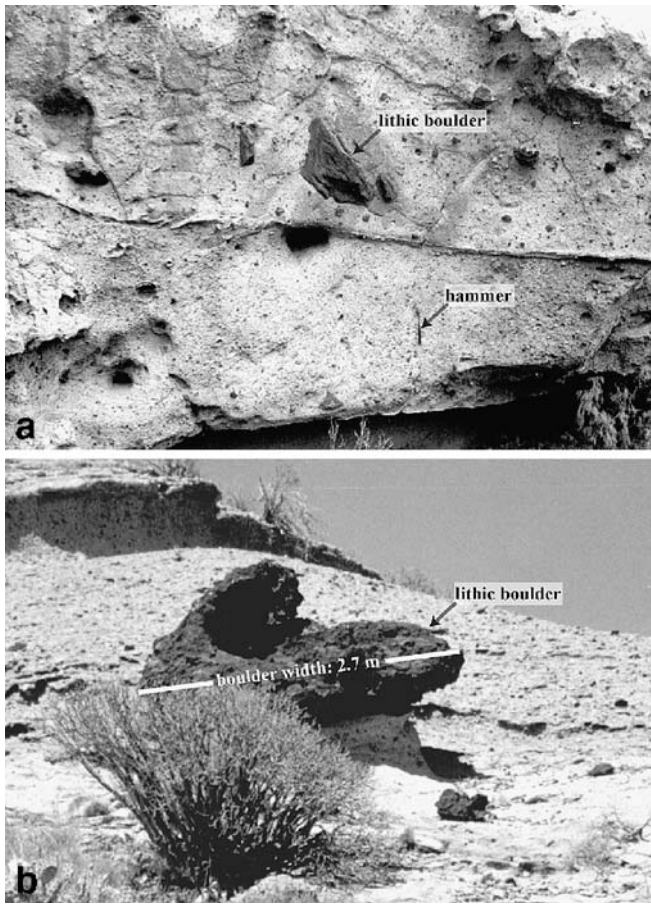
Fig. 3 Examples of large basalt lithic boulders within the Abrigo Ignimbrite at **a** Locality 178, and **b** Locality 204

described above and consists of (1) a lower thin fine ash layer (Eras-A unit), (2) four successive thick depositional units of massive, lithic-rich ignimbrite (Eras-B to –E units), the upper two which contain concentration zones of vent-derived lithic cobbles and boulders, possibly correlating to the upper Sur-A unit, and (3) two upper thin deposits of fine ash (Eras-F unit) and coarse ash (Eras-G unit), one or

both being possible correlatives of the Sur-C unit. (Pittari 2004; Pittari et al. 2006; Fig. 2b). Large basalt boulders used in this study occur throughout the Eras-C unit (Figs. 2b and 3a). The barranco has relatively steep slopes and had a similar topography prior to the Abrigo eruption, based on measurements of dip and strike at the base of the deposit, which suggest that the palaeoslope varied from 25 to 30°. Gentler palaeoslopes (<10°) occur on the adjacent ridges and about 500 m upstream of the barranco. The source basalt for the accidental boulders crops out in the walls and upstream of the barranco.

The second site is within the Barranco del Tapado, north of the main airport, about 3 km from the coast. Here, the Abrigo Ignimbrite is up to 12.5 m thick and the Sur-A, -B and –C units are present (Fig. 2b). Large boulders used in this study occur near the top of the Sur-A unit (1) in a monolithologic lithic concentration zone of highly porphyritic basalt on the western wall of the barranco (Loc. 203, Fig. 1) and (2) as a large boulder of vesicular basalt on the eastern wall (Loc. 204, Figs. 1 and 3b). Mono- and bilithologic concentration zones of vesicular basalt and dense, glassy, juvenile clasts, not used here, are also present in the lower Sur-C unit. Palaeoslopes in this region were generally less than 10°, although locally they were up to 25°. The source rocks are exposed at the base, and upstream of the barranco.

Theory

An object at rest on a surface will begin to move when the external forces acting on it are large enough to overcome the force of static friction between it and the surface. The minimum applied force, F, required to move a boulder with mass, m, resting on a slope of angle, θ, is represented diagrammatically in Fig. 4a and is given by:

$$F = \mu_s mg \cos \theta - mg \sin \theta \qquad (1)$$

a   **b**
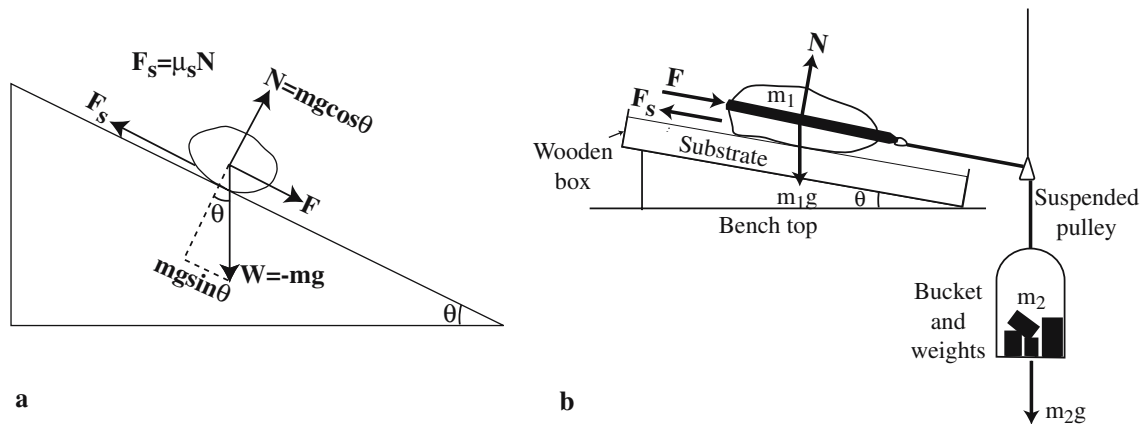
Fig. 4 a Forces acting on a boulder of mass, m, at rest on a slope at an angle, θ, and a coefficient of static friction, μ_s, just prior to sliding under an external applied force, F. N, normal force; W, weight of boulder; F_s, force of static friction; g, gravitational acceleration. **b** Basic generalised design of the static friction experiments (see main text and Appendix) in which an applied force is exerted on the boulder, with mass m_1, by the measured weight of an object of mass, m_2

where μ_s is the coefficient of static friction between the boulder and the substrate and g is gravitational acceleration (9.8 m s^{-1}).

The applied force exerted on the boulder by a pyroclastic flow is the force of aerodynamic drag, D, which is given by:

$$D = 0.5 C_D \rho V^2 A \qquad (2)$$

where ρ and V are the density and velocity of the flow parallel to the surface, respectively, A is the cross-sectional area of the boulder over which the force is applied and C_D is the coefficient of aerodynamic drag. Dynamic pressure, P, is that part of Eq. (2) that represents the properties of the flow:

$$P = 0.5 \rho V^2 \qquad (3)$$

The drag force and dynamic pressure within a pyroclastic flow varies over space and time as a result of the complex variation in flow density and velocity. This study is concerned with the minimum drag force required to just move the large boulders observed within the Abrigo ignimbrite deposit (i.e. when D equals F). The value represents a minimum instantaneous local drag force. A boulder, once entrained into the bedload of a pyroclastic flow, may come to rest onto the substrate several times during its transport period. A drag force of similar magnitude to the initial force is required each time to overcome the resulting static friction. In addition, the initial drag force is likely to be comparable to the drag force on the boulder at the instant before it is deposited at its final location.

Assumptions

Pyroclastic flows are complex and may contain localised or larger scale vertical and horizontal gradients in bulk flow velocity and density (Druitt 1992, 1998; Palladino and Valentine 1995) or variations in flow direction. Generally towards the flow-substrate boundary there is a decrease in velocity and an increase in density (Druitt 1992, 1998; Palladino and Valentine 1995). These variations, along with topographic irregularities and interaction of the flow with the boulder, may create varying degrees of turbulence.

For simplicity, these complexities are generalised by considering the drag force as an average force over the frontal area of the boulder, and that it acts perpendicular to this area.

Pyroclastic flows are here viewed as high particle concentration gas-charged granular flows consisting of a poorly sorted mixture of fine ash to boulder-sized grains and interstitial gas. The approximation to fluid dynamic principles described here (i.e. drag law) breaks down as increasingly finer scales are considered and grain-grain interactions become more important. However, this study considers processes on the scale of large boulders (10–100 s of centimetres) whereby the surrounding fine ash-gas mixture is approximated as a single-phase dynamic fluid which can exert a drag force on the boulders.

The coefficient of aerodynamic drag, C_D in Eq. (2), depends on the particle Reynolds number, Re, and the shape of the boulder. For circular disks, plates and cylinders within flows of moderate Reynolds numbers ($\approx 50 < \text{Re} < 4 \times 10^5$), C_D is approximately constant with a value of about 1.1 (e.g. Panton 1996; Massey 1998; Barlow et al. 1999; Clarke and Voight 2000). C_D for spheres under the same flow conditions is approximately 0.5 (Massey 1998). The angular, polygonal surface of the boulders over which the drag force is applied approximates a shape somewhere between a sphere and a flat disk or plate. A value for C_D of 0.8 has been chosen as a reasonable estimate for this study, however, further research on drag coefficients specific to the dense objects in pyroclastic density currents is required to improve the accuracy of dynamic pressure estimates.

The flow conditions in the lower part of a pyroclastic flow are likely to fall within the range of Reynolds numbers for which these values of C_D are valid (i.e. $\sim 50 < \text{Re} < 4 \times 10^5$). Laminar flow conditions, represented by lower Reynolds numbers (<500, e.g. Cas and Wright 1987), may occur near the flow-substrate boundary, but are unlikely to occur over the whole surface of the boulder. Higher Reynolds numbers indicative of high degrees of turbulence are also unlikely due to high particle concentrations and relatively low flow velocities in the basal zone of the flow. Hence, an intermediate flow regime, between laminar and highly turbulent, is assumed here (cf. Wohletz 1998).

The original orientation of the boulder relative to the substrate and to the flow direction is likely to affect the nature of its initial motion. It also affects the frontal area, A, of the boulder over which the drag force is applied. A non-

Fig. 5 The effect of boulder orientation **a** relative to the substrate and **b** relative to the direction of flow. D, drag force; F_s, force of static friction; A, cross-sectional area of boulder perpendicular to flow
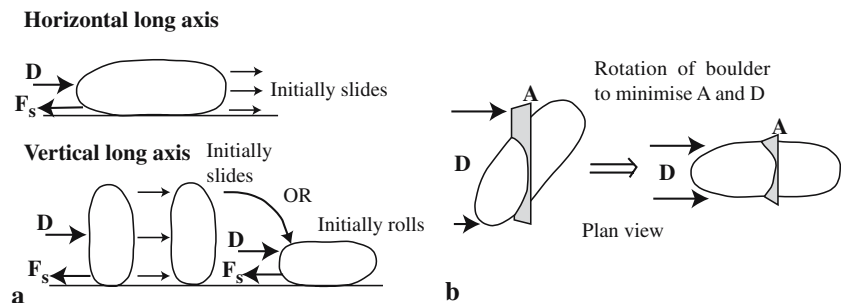
equidimensional boulder on the surface may lie with its long axis parallel (flat) or perpendicular (upright) to the substrate (Fig. 5a), or even at an angle to the substrate. In the first case, the drag force is most likely to cause the boulder to initially slide along the substrate. The upright boulder, although it experiences a higher drag force due to the larger frontal area, is relatively unsteady with respect to its weight. It will either slide or roll initially. However, if it rolls over without significant momentum it will be re-oriented into the horizontal position where it will be required to slide. Probabilistically, most loose boulders will lie in the more stable horizontal position, although upright boulders are possible in some cases (e.g. columnar basalt). Hence, the initial motion in the direction of flow for most boulders is by sliding.

Before sliding forward, however, a boulder is likely to rotate so that its long axis is oriented parallel to the direction of flow (Fig. 5b). This minimises the drag force required to push it by reducing the frontal area, A. The drag force will still need to overcome the static frictional force before it can push the boulder forward. Hence, when calculating the minimum drag force required to initially push the boulder, only the minimum frontal area is considered.

The relationship between the boulder and the substrate prior to its displacement by the flow is uncertain, however, some reasonable assumptions can be made. Several possible scenarios on Tenerife are considered (Fig. 6). The boulder could have been a fragment broken off from a larger basaltic body (case 1) or was loose on the ground. If it was a loose boulder, it may have been lying on a smooth (case 2) or rough (case 3) rock surface, or on a loose fine-grained soil/ash (case 4), or coarser-grained scree deposit (case 5). The boulder may have been partially buried within soil or scree (case 6) or shielded by a topographic obstacle (case 7). Combinations of these scenarios are also possible.

Since this study involves the minimum drag force required to move a boulder of a particular size, cases 1, 6 and 7 are not considered. For cases 2–5, the minimum force depends on μ_s between the boulder and the surface.

Appropriate values for μ_s to accommodate the range of boulder-substrate surfaces have been determined experimentally (see below). It is assumed that μ_s remains constant over time before the boulder begins to move, although in reality, flow erosion or accumulation of substrate material around and in front of the boulder, respectively and buoyancy forces are likely to affect μ_s. However, given the large size and mass of the boulders, these effects are considered to be minor.

Experimental data

Coefficients of static friction, although routinely determined in rock mechanics and geotechnical studies, are either very generalised or specific to individual problems. A series of simple experiments (experiments 1–4, Tables 1 and 2; Fig. 4b; Appendix) were run to determine an appropriate value of μ_s between the boulders and substrate use in this study and involved determining the minimum force, represented by the gravitational force on a measured mass, m_2, required to initiate motion of a boulder of mass, m_1, on a given substrate. Details of the experimental method are described in the Appendix and Fig. 4b. μ_s was determined for five boulders (A-E) of different masses and degrees of surface roughness (surfaces X, Y and Z of boulder D) on both soil and concrete substrates and on various slope angles. Concrete and soil was used to represent typical rock and loose sediment/soil/ash substrates, respectively, on Tenerife.

Results

The results of experiments 1 to 4 are shown in Tables 1 and 2. Instrumental errors are quoted for m_1, m_2 and μ_s. For each run of five repeated measurements the average μ_s, standard error and standard error in the mean have been quoted.

There are no significant systematic variations in μ_s between boulders of different mass and between different slope angles, as expected. Variations in μ_s are a result of the nature of the contact surfaces between the boulder and the substrate. Boulders A, B, C and D have a slightly higher μ_s on concrete than on soil, although boulder E has comparable results, within error, for both types of substrate. Internal friction and shearing within the soil may play a part in reducing the overall static friction between the boulder and soil hence lowering μ_s. On soil substrates lower μ_s values resulted from rougher contact surfaces on a given boulder. Rougher surfaces are likely to penetrate deeper into the soil thus being influenced more by the internal friction of the soil, which acts to lessen the overall apparent friction.

Case 1: Boulder dislodged from outcrop

Joint block

Rock jag

Outcrop

Case 2: Loose boulder on smooth rock surface

Fresh rock

Case 3: Loose boulder on rough rock surface

Fresh rock

Case 4: Loose boulder on fine-grained soil

Fine-grained soil

Case 5: Loose boulder on coarse-grained scree

Coarse-grained scree

Case 6: Loose boulder partially buried within soil or scree

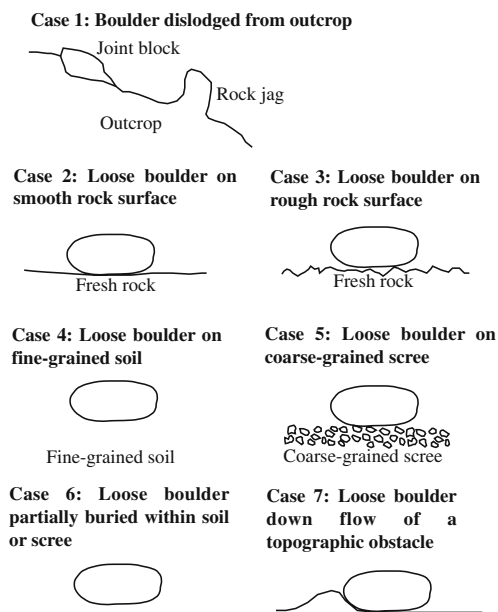**Case 7: Loose boulder down flow of a topographic obstacle**

Fig. 6 Various possible scenarios concerning the relationship between the boulder and substrate prior to entrainment into the pyroclastic flow

Table 1 Results of coefficient of friction experiments 1 and 2 (Units of m_1 and m_2 are kilograms; μ_s is unitless; Av average)

	Boulder A m_1 39.95		Δm_1 0.025		Boulder B m_1 19.95		Δm_1 0.025		Boulder C m_1 11.05		Δm_1 0.025		Boulder D m_1 8.35		Δm_1 0.025		Boulder E m_1 3.75		Δm_1 0.025	
Trial	m_2	Δm_2	μ_s	$\Delta\mu_s$	m_2	Δm_2	μ_s	$\Delta\mu_s$	m_2	2	$\mu_{>s}$	$\Delta\mu_s$	m_2	Δm_2	μ_s	$\Delta\mu_s$	m_2	Δm_2	μ_s	$\Delta\mu_s$
Experiment 1: Varying boulder type (A-E, see Appendix) on a soil substrate; angle of slope, 0°; contact surface X (see Appendix)																				
1	28.45	0.125	0.712	0.003	14.65	0.075	0.734	0.004	7.40	0.125	0.670	0.011	5.50	0.125	0.659	0.015	2.85	0.125	0.760	0.034
2	26.75	0.175	0.670	0.004	13.45	0.100	0.674	0.005	7.45	0.125	0.674	0.011	6.50	0.125	0.778	0.015	3.25	0.075	0.867	0.021
3	24.45	0.175	0.612	0.004	14.10	0.100	0.707	0.005	7.20	0.125	0.652	0.011	5.45	0.100	0.653	0.012	3.15	0.075	0.840	0.021
4	25.40	0.125	0.636	0.003	13.70	0.175	0.687	0.009	6.95	0.100	0.629	0.009	6.35	0.075	0.760	0.009	3.05	0.075	0.813	0.021
5	25.25	0.125	0.632	0.003	14.55	0.075	0.729	0.004	6.60	0.100	0.597	0.009	5.75	0.075	0.689	0.009	3.30	0.075	0.880	0.021
Av.			0.652				0.706				0.644				0.708				0.832	
σ_{n-1}			0.039				0.026				0.032				0.058				0.048	
σ_m			0.018				0.012				0.014				0.026				0.021	
Experiment 2: Varying boulder type (A-E, see Appendix) on a concrete substrate; angle of slope, 0°; contact surface X (see Appendix)																				
1	29.35	0.125	0.735	0.003	14.65	0.125	0.734	0.006	7.95	0.125	0.719	0.011	6.15	0.125	0.737	0.015	3.35	0.125	0.893	0.034
2	27.50	0.150	0.688	0.004	16.00	0.075	0.802	0.004	7.50	0.150	0.679	0.014	6.00	0.125	0.719	0.015	3.00	0.125	0.800	0.034
3	26.15	0.425	0.655	0.011	14.35	0.425	0.719	0.021	7.65	0.125	0.692	0.011	6.65	0.125	0.796	0.015	2.90	0.175	0.773	0.047
4	26.30	0.125	0.658	0.003	15.10	0.125	0.757	0.006	8.90	0.100	0.805	0.009	5.20	0.100	0.623	0.012	3.15	0.125	0.840	0.034
5	28.85	0.150	0.722	0.004	14.40	0.150	0.722	0.008	7.70	0.100	0.697	0.009	5.75	0.100	0.689	0.012	2.65	0.150	0.707	0.040
Av.			0.692				0.747				0.719				0.713				0.803	
σ_{n-1}			0.036				0.034				0.051				0.064				0.070	
σ_m			0.016				0.015				0.023				0.029				0.031	

Table 2 Results of experiments 3 and 4 (Units of m_1 and m_2 are kilograms; μ_s is unitless; Av average)

	Experiment 3: Varying the slope angle using boulder D with contact surface X (see Appendix) in contact with a soil substrate[a]											
	10°				15°				20°			
Trial	m_2	Δm_2	μ_s	$\Delta\mu_s$	m_2	Δm_2	μ_s	$\Delta\mu_s$	m_2	Δm_2	μ_s	$\Delta\mu_s$
1	3.65	0.125	0.620	0.021	3.90	0.075	0.751	0.015	2.40	0.075	0.670	0.021
2	4.15	0.075	0.681	0.012	3.30	0.075	0.677	0.016	1.80	0.100	0.593	0.033
3	4.25	0.125	0.693	0.020	2.85	0.075	0.621	0.016	2.00	0.100	0.619	0.031
4	4.45	0.100	0.717	0.016	3.10	0.100	0.652	0.021	1.75	0.075	0.587	0.025
	3.75	0.075	0.632	0.013	3.05	0.100	0.646	0.021	2.30	0.100	0.657	0.029
Av.			0.669				0.670				0.625	
σ_{n-1}			0.041				0.050				0.037	
σ_m			0.018				0.022				0.017	
	Experiment 4: Varying surface of boulder D (surfaces X, Y, Z see Appendix) in contact with a soil substrate; angle of slope, 0°[a]											
					Surface Y				Surface Z			
1					4.80	0.075	0.575	0.009	5.20	0.100	0.623	0.012
2					5.00	0.075	0.599	0.009	5.30	0.125	0.635	0.015
3					5.85	0.150	0.701	0.018	5.50	0.100	0.659	0.012
4					4.85	0.075	0.581	0.009	5.30	0.100	0.635	0.012
5					4.90	0.125	0.587	0.015	5.10	0.100	0.611	0.012
Av.							0.608				0.632	
σ_{n-1}							0.052				0.018	
σ_m							0.023				0.008	

[a]Experiment 1 (Table 1) contains the results for a slope angle of 0° and for surface X under the same conditions in experiments 3 and 4 respectively

The averages of all μ_s values for soil (experiments 1, 3 and 4, Tables 1 and 2) and concrete (experiment 2, Table 1) substrates, respectively are:

$$\mu_s(\text{soil}) = 0.675 \text{ and } \sigma_{n-1}(\text{soil}) = 0.072$$

and

$$\mu_s(\text{concrete}) = 0.734 \text{ and } \sigma_{n-1}(\text{concrete}) = 0.062.$$

Both μ_s(soil) and μ_s(concrete) are within error of each other and it is not necessary to treat them separately for further calculations of dynamic pressure. Hence, a representative value of μ_s expected between large boulders within the Abrigo ignimbrite and the original substrate (either soil, ash or fresh rock) they were resting on is obtained from the average of all values of μ_s (experiments 1–4; Tables 1 and 2):

$$\mu_s = 0.695 \text{ and } \sigma_{n-1} = 0.074$$

This value is used here for further dynamic pressure calculations.

Field data

Large boulders within the Abrigo Ignimbrite at the two localities described above were approximated to a simple shape of best fit and their dimensions measured with a tape measure to determine volume and minimum cross-sectional area (Fig. 7). The six largest boulders within the Eras-C unit at Locality 178 (boulders A-F) were measured to determine the highest minimum drag force throughout the entire depositional period. In addition, the eight largest boulders at a single stratigraphic level, 5–7 m above the base of the Eras-C unit, were measured (boulders G-N) to assess the minimum drag force during a more restricted length of time. Four of these boulders (K-N) were not fully exposed limiting the measurement of all dimensions. However, they appeared to be approximately equant in at least two dimensions and a square surface was assumed. The four largest boulders within the Sur-A LCZ at Locality 203 were measured along with the very large boulder within the Sur-C unit at Locality 204.

Samples of the boulders were collected at each locality (massive basalt, Loc. 178; vesicular basalt, Loc. 204; ankaramite, Loc. 203) and their density determined first by weighing each sample then measuring their volume by observing the amount of water displaced by each sample within a beaker.

Assumptions

Boulder shape and surface roughness are likely to affect the values used for both C_D and A in Eq. (2), μ_s in Eq. (1) and also in determining the volume of each boulder. Accidental basalt boulders within the Abrigo ignimbrite are generally subangular to angular and display complex shapes with randomly sized and oriented polygonal or curved surfaces.

Fig. 7 Approximate shapes and measured dimensions (quoted in centimetres) of lithic boulders, labelled A to S, used in this study. The minimum cross-sectional area, *A*, over which the drag force is applied is shaded *grey*

Barranco de la Cera (Locality 178)

6 largest boulders within the Eras-C unit.
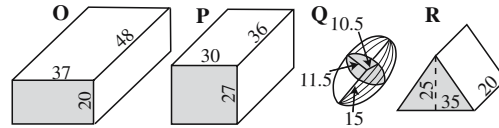(massive basalt)
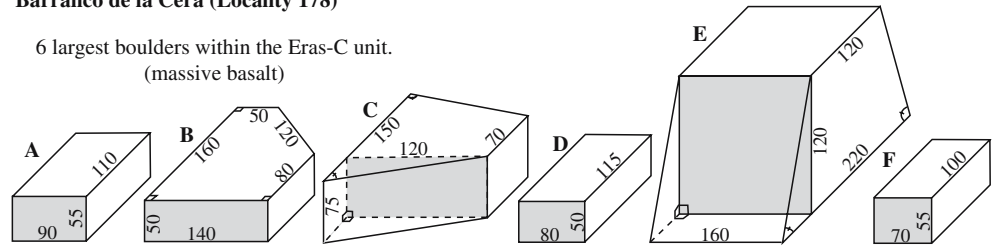
8 largest boulders at the same stratigraphic level, 5-7 m above the base of the Eras-C unit.
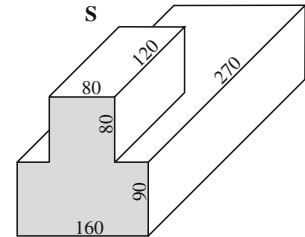(massive basalt)
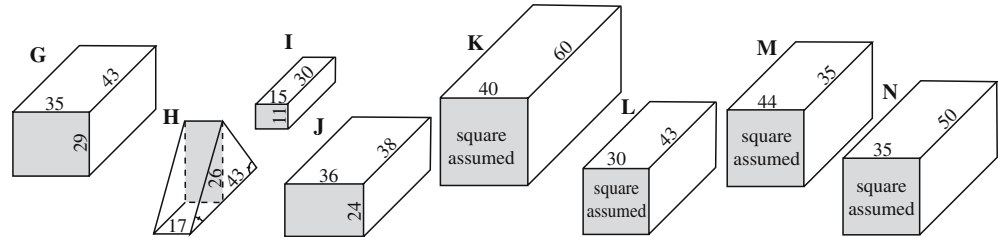
Barranco del Tapado (North of Airport): western wall (Locality 203)

4 largest boulders in a lithic concentration zone (upper Sur-A unit).
(ankaramite)

Barranco del Tapado (North of Airport): eastern wall (Locality 204)

Large boulder near the base of the Sur-C unit.
(vesicular basalt)

Individual surfaces contain a significant degree of roughness. The shape of each boulder was approximated to a simple prism or ellipsoid with smooth surfaces to simplify the measurement of dimensions.

The size and density of each boulder was used to calculate its mass. The approximation to simple shapes creates an error in determining its real volume, however, a visual "best-fit" shape was applied to each boulder. Boulder densities are based on density measurements of small samples of each lithology. Density of a small sample does not take into account larger density variations throughout the boulder, particular with vesicular lithologies. The values of volume, density and resultant mass are still likely to represent the true properties of the boulder to within an estimated error of about 10%.

If the angle of the slope, θ, on which the boulder rests increases, the component of the weight force parallel to the slope also increases. This reduces the minimum drag force required to move the boulder. A maximum slope angle will occur when the boulder moves under its own weight without any applied force. This condition occurs when:

$$\mu_S = \tan \theta \qquad (4)$$

At the Barranco del Tapado site and on the ridges and upslope of the Barranco de la Cera, palaeoslopes are generally less than 10°, and Eq. (1) can be simplified as follows:

$$\sin \theta \approx 0, \ \cos \theta \approx 1 \ \text{and} \ F = \mu_S mg \qquad (5)$$

A palaeoslope of 27° is also considered to represent the average palaeoslope of the walls of the Barranco de la Cera. Boulders could also have been entrained on gentler slopes (<10°) on the adjacent interfluves, further upstream and on the barranco floor. An increase in slope may act as a hydraulic jump causing a pyroclastic flow to bypass the steep slope, hence entrainment of boulders could be limited to the relatively gentle top and foot of the slope.

Results

Table 3 lists the density, volume, mass and minimum cross-sectional area of each boulder (A-S, Fig. 7) and subsequently the minimum dynamic pressure required to move the boulder on a slope angle of <10°, and additionally, for the Barranco de la Cera, a slope angle of 27°. The values used for μ_s and C_D are 0.695 and 0.8 respectively, as discussed above.

Discussion

Dynamic pressures in pyroclastic density currents have been estimated from blown-down poles and trees (Clarke and Voight 2000) or by comparing damage to buildings (Valentine 1998; Nunziante et al. 2003; Baxter et al. 2005; Table 4). The minimum dynamic pressures required to move the large boulders described in this study are comparable to those from previous studies, summarised

here in Table 4, which suggests that this method compares well with previously used methods to estimate dynamic pressures in pyroclastic flows. Values calculated in this study for the Abrigo Ignimbrite pyroclastic flows range from 5 to 38 kPa for slopes of <10° to 1.1 to 9 kPa for slopes of 27°.

A significant problem with this method is the lack of information on the initial location of the boulder and the nature of the substrate it was resting on. The minimum dynamic pressure will have varied substantially depending on the angle of slope. While it is reasonable to assume that the slopes around the Barranco del Tapado are less than 10°, the palaeotopography within the Barranco de la Cera is more complex. Although the exact location of the source of the boulders for this site is not known, using the slope value of 27° is considered to give a reasonable constraint on the slope angle of the source area based on examining the nature of the preserved palaeotopography in the Barranco de la Cera. It has been shown that reasonable assumptions can be made for other parameters involved, in particular the

Table 3 Dynamic pressures, P (kilopascals), using Eqs. (1 and 2), required to move each boulder on slope angles (θ) less than 10° and, also, in the case of the Barranco de la Cera, of 27°

Sampling specification, boulder	Volume	(m)	A	P (kPa)	
	$(10^{-4}\ m^3)$	(kg)	$(10^{-4}\ m^2)$	$\theta < 10°$	$\theta = 27°$
Locality 178, Eras-C unit					
Largest boulders in unit					
Massive basalt-density: 2,610 kg m^{-3}					
A	5,445.0	1,421	4,950	24	6
B	9,400.0	2,453	7,000	30	7
C	9,900.0	2,584	9,000	24	6
D	4,600.0	1,201	4,000	26	6
E	32,640.0	8,519	19,200	38	9
F	3,850.0	1,005	3,850	22	5
Boulders at 5–7 m above base of Eras-C unit					
Massive basalt-density: 2,610 kg m^{-3}					
G	436.5	114	1020	10	2.3
H	95.0	25	440	5	1.1
I	49.5	13	170	6	1.5
J	328.3	86	860	8	2.0
K	960.0	251	1600	13	3.2
L	387.0	101	900	10	2.3
M	677.6	177	1940	8	1.8
N	612.5	160	1230	11	2.6
Locality 203, Sur-A upper LCZ					
Largest boulders in LCZ					
Ankaramite-density: 2,930 kg m^{-3}					
O	355.2	104	740	12	
P	291.6	85	810	9	
Q	75.9	22	380	5	
R	87.5	26	440	5	
Locality 204, Lower Sur-C Unit					
Large boulder					
Vesicular basalt-density: 1,800 kg m^{-3}					
S	46560.0	8381	20800	34	

Density, volume, mass (m) and minimum cross-sectional area (A) of each boulder is also shown. *LCZ* lithic concentration zone

Table 4 Summary of previously calculated dynamic pressures, compared with those for the Abrigo Ignimbrite pyroclastic flows (this study)

Eruption	Dynamic pressure range (kPa)
Abrigo eruption (this study)	1.1–38
Mt. Unzen (June, 1991)	1.9–8.0[a]
Mt. St. Helens (May, 1980)	40–43[a]
Mt. Lamington (1951)	1.3–24[a]
	7–20[b]
Merapi Volcano (22 Nov, 1994)	0.4–2.2[a]
Soufriere Hills, Montserrat (June-Dec, 1997)	1–5, up to >25[c]
Mt. Pelée, Martinique (8 May, 1902)	5–10, up to 25[c]
Mt. Pelée, Martinique (20 May, 1902)	30–70[b]
	5–9, up to >25[c]
Mt. Vesuvius, Herculaneum (AD 79)	20–70[b]
Mt. Vesuvius, Terzigno-Vesuvio (AD 79)	1–5[d]

[a]Clarke and Voight (2000)
[b]Valentine (1998)
[c]Baxter et al. (2005)
[d]Nunziante et al. (2003)

coefficients of static friction and aerodynamic drag. Other assumptions about the orientation of the boulder and its position with respect to the substrate have been made so as to minimise the predicted dynamic pressures.

Buoyant lift forces within a pyroclastic flow and their effect in reducing the static friction coefficient have been ignored in this study. However, the large forces required to lift heavy boulders are probably comparable to, if not greater than, the drag force in the direction of flow. The dynamic pressures calculated in this study are still likely to be minimum values.

Dynamic pressure can be used to obtain an idea of the bulk density and velocity of a pyroclastic flow. Bulk density cannot be observed directly or measured, however, its value must be between that of the pure gas phase (e.g. air: 1.2 kg m^{-3}) and that of the ash deposit. Mt. St. Helens pyroclastic flow deposits of July 22 and August 7, 1980 were observed on August 12 to have a bulk density of 1,450 kg m^{-3} for channel deposits and 550–1,050 kg m^{-3} for pumiceous levee deposits (Wilson and Head 1981).

Estimates of bulk flow density have been based on fundamental assumptions of the pyroclastic flow properties. Sparks (1976) assumed that pyroclastic flows were dense and poorly expanded and estimated a flow bulk density of 1,220 kg m^{-3} for an ignimbrite deposit near Sorano, Vulsini, about 80% of the deposit density (1,550 kg m^{-3}). Wilson (1985) estimated minimum flow densities for the Taupo ignimbrite of 300–600 kg m^{-3} based on the density of buoyant pumice clasts. Martini (1996) assessed the pyroclastic flow that destroyed Pompeii (AD 79) and calculated bulk densities from 95 to 220 kg m^{-3} based on particle volumetric fractions between 5 and 10%. Smaller bulk densities of 3.4–8.3 kg m^{-3}

were calculated by Clarke and Voight (2000) for several different pyroclastic flow systems under the assumption of particle volumetric fractions between 0.0013 and 0.0032.

Pyroclastic flow velocities are measurable and quoted values are more reliable. Typical flow front velocities of 10–60 m s^{-1} (36–216 km h^{-1}) have been observed for small volume pyroclastic flows around Soufriere Hills, Montserrat (Cole et al. 1998; Calder et al. 1999; Loughlin et al. 2002). Pole and tree blow-down measurements have revealed flow velocities of 27–78 m s^{-1} (97–281 km h^{-1}) for some recent eruptions and up to 110–130 m s^{-1} (396–468 km h^{-1}) for the 1980 Mt. St. Helens eruption (Clarke and Voight 2000). Model predictions of larger volume pyroclastic flows with an average grainsize of 1 mm suggest that the flow velocity ranges from 10 to 150 m s^{-1} (36–540 km h^{-1}) for eruption rates of 10^8–10^{10} kg s^{-1} (Bursik and Woods 1996).

Given the range in minimum instantaneous dynamic pressure calculated for the Abrigo pyroclastic flow, and using a range of possible bulk flow densities previously cited (see above), the range in minimum bulk flow velocity was calculated and summarised in Table 5. Minimum bulk flow velocities calculated for the Abrigo pyroclastic flow (Table 5) are comparable to the range in velocities estimated for other pyroclastic flow systems (Table 4). If the basal zone of the pyroclastic flow had a high particle concentration, near that of the resulting deposit (e.g.

Table 5 Estimates of the range of bulk velocities for the Abrigo pyroclastic flows, given the calculated range of dynamic pressures (P) and the range of possible bulk densities cited within the literature[a]

Abrigo calculated P (kPa)	Possible flow bulk density above depositional boundary layer (kg m^{-3})[a]	Resultant required velocity for Abrigo pyroclastic flow (m s^{-1})
1.1	A: 10	15
	B: 700	1.8
	C: 1400	1.3
10	A: 10	45
	B: 700	5.3
	C: 1400	3.8
20	A: 10	63
	B: 700	7.6
	C: 1400	5.3
30	A: 10	78
	B: 700	9.3
	C: 1400	6.5
38	A: 10	87
	B: 700	10
	C: 1400	7.4

[a]'A' approximates the minimum bulk density similar to values quoted by Clarke and Voight (2000) and only just greater than the density of air (1.2 kg m^{-3}). 'B' represents an intermediate bulk density, which is only slightly greater than densities quoted for the Taupo Ignimbrite (300 to 600 kg m^{-3}, Wilson 1985). 'C' approximates the maximum bulk density, which is near the density of channel deposits quoted at Mt. St. Helens (Wilson and Head 1981)

1,400 kg m^{-3}, cf. Wilson and Head 1981), then only relatively low minimum velocities, from 1.3 to 7.4 m s^{-1} (4.7–27 km h^{-1}), would have been required to move the boulders. Alternatively, a basal zone with a bulk density not much greater than for air (cf. Clarke and Voight 2000), would have required relatively higher minimum velocities, from 15 to 87 m s^{-1} (54–313 km h^{-1}).

Small boulders on flat surfaces require at least 5–13 kPa to be moved (Table 4). These dynamic pressures are most likely correct for the Barranco del Tapado where the slope angle is well constrained. In addition, the small boulders occur within a planar lithic pebble to boulder concentration zone, hence these dynamic pressures were likely to have been consistent throughout the local pyroclastic flow system when these boulders were entrained. Minimum dynamic pressures obtained from the small boulders at the same stratigraphic level within the Barranco de la Cera could also represent more general flow conditions.

Large isolated boulders are less common and are likely to have required highly localised instantaneous dynamic pressures. An analogy is that of high speed wind gusts within a storm. On flat slopes large boulders require high dynamic pressures (22–38 kPa) to be moved. Alternatively, the large boulders could have been resting on steeper slopes and would have only required dynamic pressures comparable to those for small boulders on flat slopes.

In trying to conceptualise the destructiveness and hazard implications of the Abrigo pyroclastic flows, it is useful to compare the range of dynamic pressures with those observed in other natural phenomena. As previously stated, small boulders probably represent more general flow conditions, although flow gusts may generate dynamic pressures high enough to move large boulders. The pyroclastic flow dynamic pressures were used to calculate corresponding flow velocities for media of air or water (Table 6). Thus comparisons could be made to hydrological and meteorological phenomena.

Typical minimum dynamic pressures (5–13 kPa) estimated for the Abrigo pyroclastic flows, which are equivalent to air and water flow velocities of 91–150 m s^{-1} and 3.2–5.2 m s^{-1}, respectively, are only comparable to or greater than those encountered in the most severe tornadoes (Fujita Scale, F4–F6; 93–169 m s^{-1}) or peak flow periods during major river floods (e.g. 1993 Mississippi major flood event; 3.4 m s^{-1}, Southard and Smith 1995). Flow gusts in pyroclastic flows (up to 38 kPa, equivalent to up to 252 m s^{-1}, air; 8.7 m s^{-1}, water) are far more powerful than any meteorological phenomena but can be compared to the current intensity at the crest of the Niagara Falls (8.9 m s^{-1}, Figler 2003).

Lahars, which are debris flows and hyperconcentrated flows proximal to volcanic edifices (Vallance 2000), are also known to transport large boulders up to 5–15 m in diameter (e.g. Mileti et al. 1991; Capra and Macías 2000; Scott et al. 2005). These indicate relatively higher dynamic

Table 6 Range of minimum instantaneous dynamic pressures within the Abrigo pyroclastic flows, bulk flow velocities for air and water with the same dynamic pressures, and a comparison to velocities of powerful meteorological and hydrological phenomena

Range of dynamic pressures in Abrigo pyroclastic flows	5–13 kPa, up to 38 kPa
Range in flow velocities for air exerting the same dynamic pressure as calculated for the Abrigo pyroclastic flows (density of air: 1.2 kg m^{-3})	91–150 m s^{-1}, up to 252 m s^{-1}
Range in flow velocities for water exerting the same dynamic pressure as calculated for the Abrigo pyroclastic flows (density of water: 1,000 kg m^{-3})	3.2–5.2 m s^{-1}, up to 8.7 m s^{-1}
Typical velocities of meteorological phenomena	
Category 5 hurricane (Saffir-Simpson scale)[a]	>70 m s^{-1}
Devastating F4 tornado (Fujita scale)[b]	93–116 m s^{-1}
Incredible tornado (F5 on Fujita scale)[b]	117–142 m s^{-1}
Inconceivable tornado (F6 on Fujita scale)[b]	143–169 m s^{-1}
Typical velocities of hydrological phenomena	
Peak flood flow (1993 Mississippi River major flood event)[c]	3.4 m s^{-1}
Crest of Niagara Falls[d]	8.9 m s^{-1}

[a] Saffir-Simpson hurricane intensity scale categorises a hurricane from 1 to 5 based on the measured wind speed
[b] Fujita scale categorises a tornado's intensity or wind speed from F1 to F6 based on the damage caused to infrastructure
[c] Southard and Smith (1995)
[d] Figler (2003)

pressures than those estimated here for the Abrigo pyroclastic flow, possibly due to their water-saturated nature. The cause of boulder entrainment into a lahar and the local topographic relief should be considered on a case by case scenario before estimating dynamic pressures using the method outlined here.

Conclusions

A new method for estimating the minimum instantaneous dynamic pressure within the basal zone of pyroclastic flows using accidental lithic boulders within ignimbrite deposits has been proposed in this study. This method can be applied to both ancient and modern lithic-rich ignimbrite deposits. The dynamic pressures estimated for the Abrigo pyroclastic flows range from 5 to 38 kPa and indicate the pyroclastic flow velocities would have been in the range of 1.3 to 87 m s^{-1}. These values are comparable to measured dynamic pressures and flow velocities of modern pyroclastic flow events.

The very large minimum dynamic pressures capable of transporting small and large boulders as well as the widespread dispersal of the Abrigo Ignimbrite emphasises the destructiveness of the Abrigo pyroclastic flow.

Appendix-Coefficient of static friction experiments

Theory and experimental method

A boulder of mass, m_1, was placed on top of a standard substrate within a raised wooden box at a slope angle, θ (Fig. 4b). It was strapped to a strong wire cord, which was threaded through a hanging pulley and connected to a bucket suspended above the ground. The bucket was loaded incrementally with small weights until the boulder moved. The bucket and its contents were then weighed. Note, however, that the actual mass which caused the boulder to move, m_2, occurs somewhere between the measured mass, x, and the difference between x and the last added incremental weight, x_i. It was assumed that:

$$m_2 = x - 0.5x_i \tag{6}$$

and the value was rounded down to the nearest 0.05 kg.

The weight of the bucket when the boulder first moves represents the minimum applied force required to overcome the force of static friction between the boulder and the substrate, F.

$$F = m_2 g = m_1 g(\mu_s \cos\theta - \sin\theta) \tag{7}$$

Hence, the coefficient of static friction is:

$$\mu_s = \frac{m_2 + m_1 \sin\theta}{m_1 \cos\theta} \tag{8}$$

When the slope is flat (i.e. θ is 0°), Eq. (8) can be simplified to

$$\mu_s = \frac{m_2}{m_1} \tag{9}$$

For each trial, the boulder was oriented so that its long axis was parallel to the applied force to simulate the likely orientation of a boulder within a pyroclastic flow. The strap was placed around the equatorial circumference of the boulder so that the force would be applied to the centre of the boulder. The wire cord between the boulder and the pulley was aligned with the long axis of the boulder and parallel to the substrate. Both the friction within the pulley and the mass of the wire cord were assumed to be negligible and the weight force of the bucket was assumed to have been transferred directly to the boulder. Unavoidable slight variations in the boulder orientation, positioning of the strap and wire cord alignment for each trial is likely to have contributed to the experimental error.

Error analysis

Each measurement of mass is limited by instrumental error. For the mass of the boulder, m_1, the error, Δm_1, consists solely of the inherent error of the scales: 0.025 kg. The error in m_2, is:

$$\Delta m_2 = \Delta x + \Delta x_i + 0.5 x_i \tag{10}$$

where, Δx and Δx_i are the inherent scale errors when weighing (1) the mass of the bucket and its contents and (2) the mass of the last incremental weight, respectively. The resultant instrumental error for μ_s, $\Delta\mu_s$, can be expressed as:

$$\frac{\Delta\mu_s}{\mu_s} = \sqrt{\left(\left(\frac{\Delta m_1}{m_1}\right)^2 + \left(\frac{\Delta m_2}{m_2}\right)^2\right)} \tag{11}$$

The effect of random errors were considered by taking five repeated measurements of m_2 for each run and determining μ_s for each value. The average μ_s, μ_s, and the standard error, σ_{n-1} was calculated for each run. The standard error represents the precision of a single measurement and is given by:

$$\sigma_{n-1} = \sqrt{\frac{\sum\limits_{i=1}^{n} \left(\mu_{s_i} - \overline{\mu}_s\right)^2}{n-1}} \tag{12}$$

where μ_{si} is a single value and n is the number of repeat measurements. Also quoted is the standard error in the mean, σ_m, which represents the increased precision due to repeated measurements.

Boulder and substrate types and their handling

Five boulders (A-E) of differing masses and surface characteristics were used for these experiments (Table 7). The surface in contact with the substrate is labelled X, although for boulder D two additional surfaces (Y and Z) were used.

Table 7 Description and mass of boulders A to E and description of the surfaces that were placed in contact with the substrate. *SE* standard error

Boulder Label	Description	Mass, m_1 (kg) (SE: +0.025 kg)	Contact surface (surface X, unless specified)	
			Area (cm²)	Description
A	Conglomerate; subrounded	39.95	740	Smooth
B	Porphyritic rhyolite; angular	19.95	510	Rough; coarsely faceted
C	Fine-grained sandstone; angular	11.05	350	Rough; coarsely faceted
D	Basalt; angular	8.35	X: 350	Smooth; fine striations
			Y: 300	Rough; coarsely faceted
			Z: 340	Fine grainy roughness
E	Basalt; angular	3.75	230	Fine grainy roughness

Two types of substrate were used: soil and concrete. Dry garden soil (50% topsoil, 50% compost) was used to represent soil, fine sediment or ash substrate on Tenerife. For each trial the soil was raked and patted lightly to maintain a consistent degree of compaction and cohesiveness. The boulder was lowered carefully onto the surface so that it did not sink greater than 3 mm into the soil. For soil/sediment substrates, the value of μ_s is a combination of the value between the rock surface and the soil and the internal friction of the soil. Variations in soil preparation and boulder placement are likely to contribute to error in μ_s.

At the instance of first motion, the boulder often dug slightly into the soil creating a mound in front of it and restricting further movement. This was overcome by adding more weight to the bucket and the final weight was considered as that which caused the boulder to move greater than 1 cm. A concrete slab to represent exposed fresh rock substrate. Grinding of the boulder on the slab after each trial slightly altered the nature of the concrete surface and may have contributed to the error in μ_s. Four experiments were conducted, each involving varying types of boulders on the two different substrates (experiment 1, soil; experiment 2, concrete), slope angle (experiment 3) and boulder contact surface (experiment 4). The details and results have been recorded in Tables 1 and 2.

References

Ablay GJ, Kearey P (2000) Gravity constraints on the structure and volcanic evolution of Tenerife, Canary Islands. J Geophys Res 105:5783–5796

Anchochea E, Fúster JM, Ibarrola E, Cendrero A, Coello J, Hernan F, Cantagrel JM, Jamond C (1990) Volcanic evolution of the island of Tenerife (Canary Islands) in the light of new K-Ar data. J Volcanol Geotherm Res 44:231–249

Barlow JB, Roe WH Jr, Pope A (1999) Low-speed wind tunnel testing, 3rd edn. Wiley, New York, pp 1–713

Baxter PJ, Boyle R, Cole P, Neri A, Spence R, Zuccaro G (2005) The impacts of pyroclastic surges on buildings at the eruption of the Soufrière Hills volcano, Montserrat. Bull Volcanol 67:292–313

Brown RJ, Barry TL, Branney MJ, Pringle MS, Bryan SE (2003) The Quaternary pyroclastic succession of southeast Tenerife, Canary Islands: explosive eruptions, related caldera subsidence, and sector collapse. Geol Mag 140:265–288

Bryan SE, Cas RAF, Martí J (1998) Stratigraphy of the Bandas del Sur Formation: an extracaldera record of Quaternary phonolitic explosive eruptions from the Las Cañadas edifice, Tenerife (Canary Islands). Geol Mag 135:605–636

Bursik MI, Woods AW (1996) The dynamics and thermodynamics of large ash flows. Bull Volcanol 58:175–193

Calder ES, Cole PD, Dade WB, Druitt TH, Hoblitt RP, Huppert HE, Ritchie L, Sparks RSJ, Young SR (1999) Mobility of pyroclastic flows and surges at the Soufriere Hills Volcano, Montserrat. Geophys Res Lett 26:537–540

Capra L, Macías JL (2000) Pleistocene cohesive debris flows at Nevada de Toluca Volcano, central Mexico. J Volcanol Geotherm Res 102:149–167

Cas RAF, Wright JV (1987) Volcanic successions: modern and ancient: a geological approach to processes, products and successions. Allen and Unwin, Sydney, pp 1–528

Clarke AB, Voight B (2000) Pyroclastic current dynamic pressure from aerodynamics of tree or pole blow-down. J Volcanol Geotherm Res 100:395–412

Cole PD, Calder ES, Druitt TH, Hoblitt R, Robertson R, Sparks RSJ, Young SR (1998) Pyroclastic flows generated by gravitational instability of the 1996-97 lava dome of Soufriere Hills Volcano, Montserrat. Geophys Res Lett 25:3425–3428

Druitt TH (1992) Emplacement of the 18 May 1980 lateral blast deposit ENE of Mt. St. Helens, Washington. Bull Volcanol 54:554–572

Druitt TH (1998) Pyroclastic density currents. In: Gilbert JS, Sparks RSJ (eds) The physics of explosive volcanic eruptions. Geol Soc Lond Spec Publ 145: 145–182

Edgar CJ (2003) The stratigraphy and eruption dynamics of a quaternary phonolitic plinian eruption sequence: the Diego Hernández Formation, Tenerife, Canary Islands (Spain). PhD Thesis, Monash University, Clayton, pp 1–264

Esposti Ongaro T, Neri A, Todesco M, Macedonio G (2002) Pyroclastic flow hazard assessment at Vesuvious (Italy) by using numerical modelling. II. Analysis of flow variables. Bull Volcanol 64:178–191

Figler RH (2003) Niagara Falls bathymetric survery. Professional Surveyor, 23(1), URL: http://www.profsurv.com/psarchiv.htm

Fuster JM, Araña V, Brandle JL, Navarro JM, Alonso U, Aparicio A (1968) Geologia y Vulcanologia de las Islas Canarias. Instituto "Lucas Mallada", CSIC, Madrid, pp 1–218

Loughlin SC, Calder ES, Clarke A., Cole PD, Luckett R, Mangan MT, Pyle DM, Sparks RSJ, Voight B, Watts RB (2002) Pyroclastic flows and surges generated by the 25 June 1997 dome collapse, Soufrière Hills Volcano, Montserrat. In: Druitt TH, Kokelaar BP (eds) The eruption of Soufrière Hills Volcano, Montserrat, from 1995 to 1999. Mem Geol Soc Lond 21:191–209

Martí J, Mitjavila J, Araña V (1994) Stratigraphy, structure and geochronology of the Las Cañadas caldera (Tenerife, Canary Islands). Geol Mag 131:715–727

Martini K (1996) Ancient Reconstruction of the Pompeii Forum: an Investigation of Seismic and Volcanic Structural Response. URL: http://urban.arch.virginia.edu/struct/pompeii/, (Nov. 29, 1997)

Massey B (1998) Mechanics of fluids, 7th edn. Stanley Thornes, Cheltenham, pp 1–722

Mileti DS, Bolton PA, Fernandez G, Updike RG (1991) The eruption of Nevado del Ruiz Volcano, Columbia, South America, November 13, 1985. National Academy Press, Washington, DC, pp 1–109

Mitjavilla J, Villa IM (1993) Temporal evolution of the Diego Hernández Formation (Las Cañadas, Tenerife) and confirmation of the age of the caldera using the $^{40}Ar/^{39}Ar$ method. Rev Soc Geol Esp 6:61–65

Nichols HJ (2001) Petrologic and geochemical variation of a caldera-forming ignimbrite: the Abrigo Member, Diego Hernández Formation, Tenerife, Canary Islands (Spain). MSc Thesis, Washington State University, Pullman, pp 1–123

Nunziante L, Fraldi M, Lirer L, Petrosino P, Scotellaro S, Cicirelli C (2003) Risk assessment of the impact of pyroclastic currents on the towns located around Vesuvio: a non-linear structural inverse analysis. Bull Volcanol 65:547–561

Palladino DM, Valentine GA (1995) Coarse-tail vertical and lateral grading in pyroclastic flow deposits of the Latera Volcanic Complex (Vulsini, central Italy): origin and implications for flow dynamics. J Volcanol Geotherm Res 69:343–364

Panton RL (1996) Incompressible flow, 2nd edn. Wiley, New York, pp 1–837

Pittari A (2004) Eruption dynamics and emplacement processes for the climactic Abrigo Member, Tenerife, Canary Islands. PhD Thesis, Monash University, Clayton, pp 1–327

Pittari A, Cas RAF (2004) Sole marks at the base of the late Pleistocene Abrigo Ignimbrite, Tenerife: implications for transport and depositional processes at the base of pyroclastic flows. Bull Volcanol 66:356–363

Pittari A, Cas RAF, Martí J (2005) The occurrence and origin of prominent massive, pumice-rich ignimbrite lobes within the Late Pleistocene Abrigo Ignimbrite, Tenerife, Canary Islands. J Volcanol Geotherm Res 139:271–293

Pittari A, Cas RAF, Edgar CJ, Nichols HJ, Wolff JA, Martí J (2006) The influence of palaeotopography on pyroclastic flow processes and facies architecture of a lithic-rich ignimbrite in a high gradient setting: the Abrigo Ignimbrite, Tenerife, Canary Islands. J Volcanol Geotherm Res 152:273-315

Scott KM, Vallance JW, Kerle N, Macías JL, Strauch JL, Devoli G (2005) Catastrophic precipitation-triggered lahar at Casita volcano, Nicaragua: occurrence, bulking and transformation. Earth Surf Process Landforms 30:59–79

Southard RE, Smith BJ (1995) Flood of 1993-Mississippi River near the Jefferson National Expansion Memorial (arch), St. Louis, Missouri. US Geol Surv Fact Sheet FS-188-95 Url: http://mo.water.usgs.gov/fact_sheets/fs-188-95-southard/report.pdf

Sparks RSJ (1976) Grainsize variations in ignimbrites and implications for the transport of pyroclastic flows. Sedimentology 23:147–188

Valentine GA (1998) Damage to structures by pyroclastic flow and surges, inferred from nuclear weapons effects. J Volcanol Geotherm Res 87:117–140

Valentine GA, Wohletz KH (1989) Environmental hazards of pyroclastic flows determined by numerical models. Geology 17:641–644

Vallance JW (2000) Lahars. In: Sigurdsson H, Houghton B, McNutt SR, Rymer H, Stix J (eds) Encyclopedia of volcanoes. Academic Press, New York, pp 601–616

Wilson CJN (1985) The Taupo eruption, New Zealand II. The Taupo ignimbrite. Phil Trans R Soc Lond A 314:229–310

Wilson L, Head JW (1981) Morphology and rheology of pyroclastic flows and their deposits, and guidelines for future observations. In: Lipman PW, Mullineaux DR (eds) The 1980 eruptions of Mount St. Helens, Washington. US Geol Surv Prof Pap 1250:513–524

Wohletz KH (1998) Pyroclastic surges and compressible two-phase flow. In: Freundt A, Rosi M (eds) From magma to tephra: modelling physical processes of explosive volcanic eruptions. Elsevier, Amsterdam, pp 247–312